Asian Monsoon Failure and Megadrought During the Last Millennium

Edward R. Cook, *et al.*

Science **328**, 486 (2010);
DOI: 10.1126/science.1185188

30. F. H. Shu, H. Shang, T. Lee, *Science* **271**, 1545 (1996).
31. F. J. Ciesla, *Science* **318**, 613 (2007).
32. A. P. Boss, *Astrophys. J.* **616**, 1265 (2004).
33. Y. J. Sheng, I. D. Hutcheon, G. J. Wasserburg, *Geochim. Cosmochim. Acta* **55**, 581 (1991).
34. This work was performed under the auspices of the U.S. Department of Energy by Lawrence Livermore National Laboratory (LLNL) under contract DE-AC52-07NA27344. Supported by NASA grants NNH07AG46I (H.A.I.) and NNH04AB47I (I.D.H.) and by LLNL grant 06-ERI-001 (J.P.B.).

Supporting Online Material
www.sciencemag.org cgi/content/full/science.1184741/DC1
Materials and Methods
SOM Text
Figs. S1 to S3
Tables S1 to S3
References

16 November 2009; accepted 16 February 2010
Published online 25 February 2010;
10.1126/science.1184741
Include this information when citing this paper.

Asian Monsoon Failure and Megadrought During the Last Millennium

Edward R. Cook,[1]* Kevin J. Anchukaitis,[1] Brendan M. Buckley,[1] Rosanne D. D'Arrigo,[1] Gordon C. Jacoby,[1] William E. Wright[1,2]

The Asian monsoon system affects more than half of humanity worldwide, yet the dynamical processes that govern its complex spatiotemporal variability are not sufficiently understood to model and predict its behavior, due in part to inadequate long-term climate observations. Here we present the Monsoon Asia Drought Atlas (MADA), a seasonally resolved gridded spatial reconstruction of Asian monsoon drought and pluvials over the past millennium, derived from a network of tree-ring chronologies. MADA provides the spatiotemporal details of known historic monsoon failures and reveals the occurrence, severity, and fingerprint of previously unknown monsoon megadroughts and their close linkages to large-scale patterns of tropical Indo-Pacific sea surface temperatures. MADA thus provides a long-term context for recent monsoon variability that is critically needed for climate modeling, prediction, and attribution.

Monsoon failures, megadroughts, and extreme flooding events have repeatedly affected the agrarian peoples of Asia over the past millennium. Despite its critical importance to human populations and ecosystems, not enough is known about the long-term spatiotemporal variability of the Asian monsoon to explain the complex mechanisms that drive its variability. A scarcity of long-term instrumental climate data for many remote regions of Monsoon Asia (*1*) (fig. S1) impedes progress toward resolving these issues. In addition, global climate models fail to accurately simulate the Asian monsoon (*2*) and related tropical Indo-Pacific forcings (*3*), and these limitations have hampered our ability to plan for future, potentially rapid and nonlinear, hydroclimatic shifts in a warming world. Under such warming, Monsoon Asia appears to be particularly vulnerable (*4*, *5*).

To better elucidate the spatial complexity of the Asian monsoon (Fig. 1A), a large-scale, spatially explicit, long-term data set is needed. Such a long-term perspective is essential both for validation of climate models and for integration and comparison with other proxy, historical, and archaeological data. This context is provided here by our Monsoon Asia Drought Atlas (MADA), which offers an absolutely dated, annually resolved reconstruction of Asian monsoon spatiotemporal variability over the past thousand years. The MADA provides a seasonal- to centennial-scale window into the Asian monsoon's repeated tendency for extended dry and wet extremes with distinct spatial flavors of response—for example, to the El Niño–Southern Oscillation (ENSO) and to Pacific Decadal Variability (*6*, *7*).

Proxy records have been produced for the past millennium for regions of Monsoon Asia and the adjacent tropical Indo-Pacific from corals (*8*), ice cores (*9*), speleothems (*10*), ocean sediments (*11*), and historical data (*12*). By their nature, these records are typically restricted by their spatial and/or temporal resolution. Many cannot provide calibration and validation estimates of reconstruction skill, and/or they do not provide the detailed land area coverage needed for resolving the Asian monsoon's complex spatiotemporal variability. Here, we used tree rings from more than 300 sites across the forested areas of Monsoon Asia to reconstruct the seasonalized Palmer Drought Severity Index (PDSI) for the summer (June-July-August) monsoon season, using a well-known, gridded measure of relative drought and wetness for the globe's land areas (*1*, *13*). The gridded reconstructions that comprise the MADA are directly analogous to the

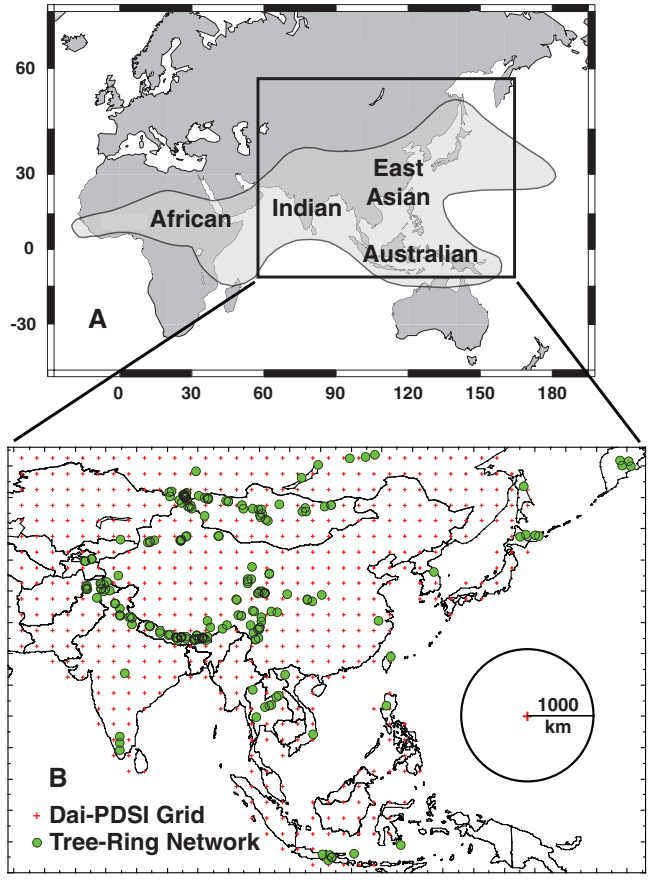

Fig. 1. (**A**) Map showing the complex regional expressions of the monsoon over Africa, India, East Asia, and south into northern Australia [redrawn from (*11*)], with the overall MADA domain enclosed by the interior black rectangle. The MADA domain limits cover all but the African portion of the greater monsoon system. (**B**) More detailed view of the MADA domain; the 534 grid points of instrumental PDSIs (*13*) (red crosses) were reconstructed by the 327-series tree-ring chronology network (*1*) (green dots). Contributors to the development of this tree-ring network are listed in table S1 (*1*).

[1]Tree-Ring Laboratory, Lamont-Doherty Earth Observatory of Columbia University, Palisades, NY 10964, USA. [2]School of Forestry and Natural Resources, National Taiwan University, Taipei 10617, Taiwan.

*To whom correspondence should be addressed. E-mail: drdendro@ldeo.columbia.edu

North American Drought Atlas (NADA) (*14*), with which it is compared below. Using this new resource, we show that monsoon failures over Asia in the modern anthropogenic period have at times been exceeded in magnitude and persistence over the past millennium, as was previously shown for megadroughts in the southwestern United States that have been linked to tropical Pacific sea surface temperature (SST) forcing (*15*).

Our Monsoon Asia reconstruction domain encompasses most of the greater Asian monsoon system (Indian, East Asian, and Australian), as well as adjacent Asian land areas to the north (Fig. 1, A and B). The 534 grid points of PDSI reconstructed for the summer monsoon season are shown in Fig. 1B, along with the network of 327 tree-ring series used for reconstruction (*1*). The latter is highly irregular relative to the PDSI grid, and its coverage is not complete because of the uneven forest cover and availability of tree species suitable for tree-ring analysis. However, using a correlation-weighted, ensemble-based modification of the "point-by-point regression" program (*1*, *14*) (figs. S5 and S6), we produced well-calibrated and validated reconstructions of summer monsoon variability over most of this domain (*1*) (fig. S7).

The MADA allows us to identify and analyze regional patterns of drought and wetness over the past millennium. This information is crucially important for identifying key modes of hydroclimatic variability that are linked to SSTs and coupled ocean/atmospheric conditions, and for providing baseline conditions for tests using climate models. Here, we used the MADA to identify the regional footprints and severity of four well-documented historical droughts: the Ming Dynasty drought (1638 to 1641) (*16*), the Strange Parallels drought (1756 to 1768) (*17*), the East India drought (1790 to 1796) (*12*), and the late Victorian Great Drought (1876 to 1878) (*18*). These comparisons also serve as validation tests of the accuracy of our reconstructed drought fields because the historical records of past drought used for comparison below are completely independent of our reconstructions and entirely predate the statistical calibration period used for reconstructing PDSI from tree rings (*1*).

The fall of the Ming Dynasty in 1644 was hastened by peasant rebellions during its final decades (*16*). Leading up to this dynastic collapse, a serious drought in the late 1630s and early 1640s appears from some historical records to have been the most severe over China for the past five centuries and may have contributed to the fall of the Ming Dynasty (*19*). Our reconstruction (Fig. 2A) shows that this drought was sharply expressed in northeastern China near Beijing, with wetter conditions prevailing toward the southeast. This pattern of reconstructed drought is similar to that of the more geographically restricted historical maps produced for the same event [figure 3 in (*19*)] and provides a more complete spatial context as compared to the historical documents.

The mid–18th-century Strange Parallels drought over Southeast Asia (Fig. 2B) coincided with a time of substantial societal upheaval and political reorganization across Southeast Asia and simultaneously across the Siberian plains (*17*). This drought was first identified from a teak ring-width record from northwest Thailand (*20*) and later corroborated in a northern Vietnamese cypress chronology (*21*). Our drought atlas reveals that much of India, particularly western India, was also affected by this multidecadal drought. This spatially broad and persistent "megadrought" from India to Southeast Asia is one of the most important periods of monsoon failure found in the MADA.

The East India drought (Fig. 2C) of 1790 to 1796 occurred during the great El Niño of the late 18th century, which was felt worldwide and resulted in widespread civil unrest and socioeconomic turmoil around the globe (*12*). Much has been made of this drought's effect in India, with several references to severe famine there (*12*), but the MADA does not suggest that it was any more severe over India than the other droughts highlighted here. Although this could be due to limited tree-ring coverage in India itself (Fig. 1B), the reconstructions over nearly all of the Indian subcontinent have significant validation skill (*1*) (fig. S7), and its more extreme occurrence in the southernmost part of India and near Sri Lanka (Fig. 2C) is consistent with historical data from those regions (*22*). It is therefore possible that this drought was not uniformly severe over India and that other nonclimatic factors may have contributed to the severity of the societal consequences (*12*). Indeed, the snow accumulation record from the Dasuopo ice core record (*23*) directly above northeastern India reveals a highly variable accumulation during this time. This suggests that the summer monsoon in that part of India was not uniformly weak during the East India drought. In contrast, the same ice core indicates more persistently below-average snow accumulation during the Strange Parallels drought period (*24*), consistent with our reconstruction that shows this earlier event to be more prolonged and severe. Dust and geochemical analysis of the Dasuopo record has been interpreted as evidence for severe drought in the late 18th century (*23*), but our atlas also indicates severe droughts to the west and north of the Himalayas, which could have been a source for dust accumulation at the ice core site during the winter monsoon. These observations demonstrate the utility of the MADA's full-field drought reconstruction feature for interpreting other point-based estimates of past hydroclimatic variability.

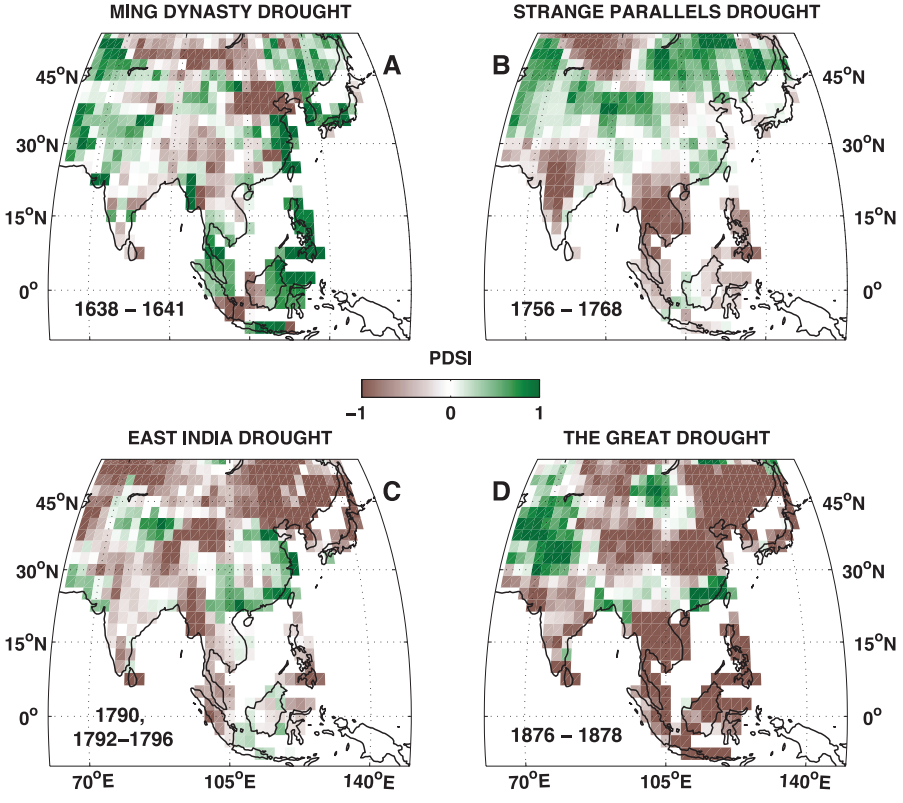

Fig. 2. Spatial drought patterns during four historical Asian droughts. Mean PDSI over each of four regional droughts identified from the historical record. (**A**) The Ming Dynasty drought (1638 to 1641) (*19*). (**B**) The Strange Parallels drought (1756 to 1768) (*17*, *20*, *21*). (**C**) The East India drought of the late 18th century (1790 and 1792 to 1796) (*12*, *22*, *23*). In 1791, much of India appears to be slightly wet, except the region around Chennai where the drought persisted (*22*). (**D**) The late Victorian Great Drought (1876 to 1878) (*18*).

The late Victorian Great Drought of 1876 to 1878 occurred during one of the most severe El Niño events of the past 150 years (*18*). The effects of this devastating drought were felt across much of the tropics (*18*) and were particularly acute in India. A revolt against the French in Vietnam also took place as a consequence of severe drought and famine at this time, and the drought was felt as far away as Jakarta, Borneo, and New Guinea (*18*). More than 30 million people are thought to have died from famine worldwide, and Colonial-era imperialism left regional societies ill-equipped to deal with the effects of drought (*18*). Our record shows that this drought was severe across nearly all areas of Monsoon Asia and ranks as the worst of the four historical droughts shown here.

The reconstruction of historic Asian monsoon failures in full spatial detail is just one application of the MADA. Underlying these broad-scale "events" are robust long-term modes of spatiotemporal variability that can provide deeper insights into the dynamics of monsoon variability over Asia. These modes are identified here through the decomposition of the full field since 1300 C.E. into Distinct Empirical Orthogonal Functions (*25*) (DEOFs, Fig. 3). The leading DEOFs are the eigenvectors of the field rotated such that they capture the maximum variance that cannot be explained by similar decomposition of a null isotropic field conditioned on the actual data (*1*). They therefore represent a compromise between the mathematical strictures of orthogonal eigendecomposition and the local patterns produced by Varimax rotation (*1*). For this reason, DEOFs may be more readily interpretable as meaningful physical modes (*25*).

Significance testing against the null field suggests that up to five leading DEOF patterns may be interpretable in the MADA. Two of these modes are highlighted in Fig. 3, with the remaining ones shown and interpreted in (*1*) (fig. S8). The leading pattern accounts for 11.5% of the total field variability, which is at least three times as large as expected from the null isotropic field. It is characterized by dominant same-sign loadings over India and Southeast Asia, with opposite sign loadings over the Tibetan Plateau, northern Pakistan, and the Pamir and Tien-Shan Mountains. The time series expansion of this mode (DPC1, Fig. 3) correlates well with the hemispherically symmetric SST anomalies characteristic of interdecadal variability in the Pacific Ocean (*7*). This DEOF pattern is associated with persistently weak monsoons in tropical south and Southeast Asia in the mid-14th and early 15th centuries (especially in the period 1351 to 1368) that are similar in timing to that of severe droughts associated with the demise of the Khmer civilization at Angkor in Cambodia (*26*). Other notable large-scale droughts also occurred in the late 16th century (1560 to 1587), at the end of the 17th century (1682 to 1699), during the Strange Parallels period (1756 to 1768), and in an apparent shift toward dry conditions after the mid-1970s (*1*) (fig. S9). Understanding the causes of these earlier droughts may help explain why a late–20th-century trend toward drier conditions and weaker monsoons has occurred over India and Southeast Asia.

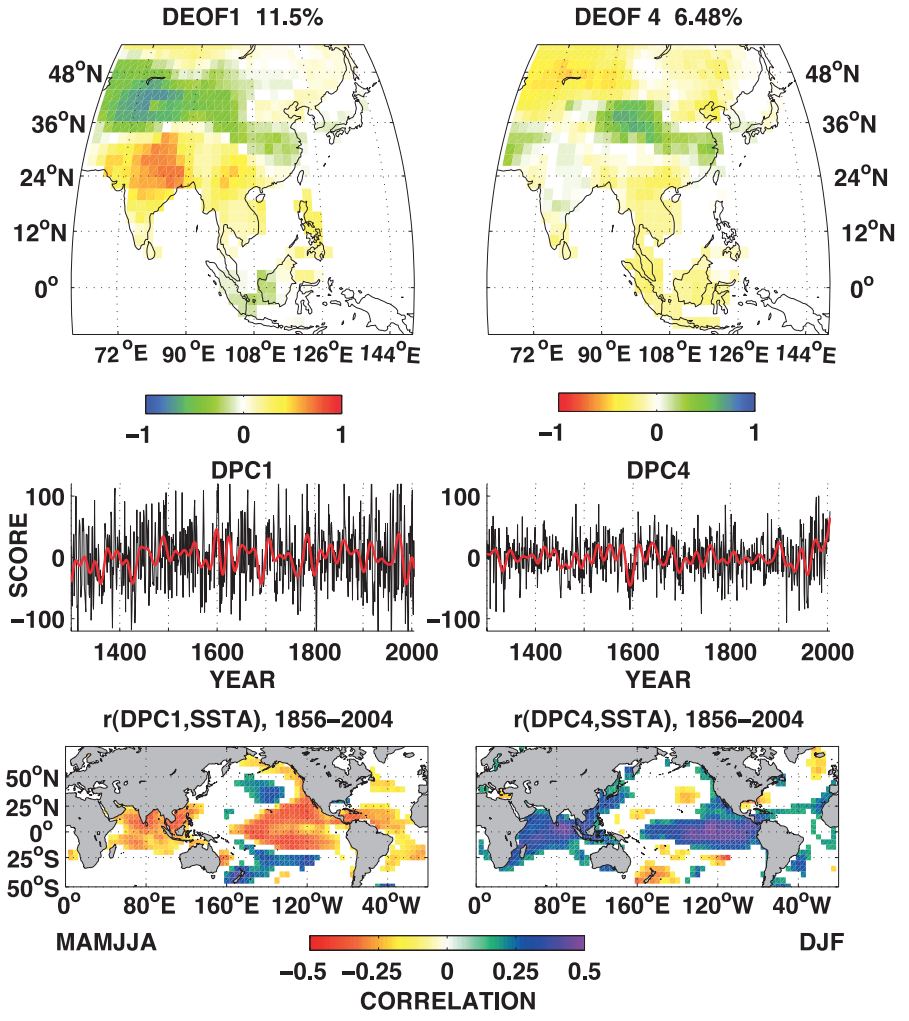

Fig. 3. Spatiotemporal patterns of the MADA since 1300 C.E. Distinct empirical orthogonal function (DEOF) (*25*) analysis of the MADA since the late Medieval period reveals five distinct modes, two of which are shown here and the remainder in (*1*). Middle panels show the time series expansion (DPCs, distinct principal components) of the corresponding spatial modes in the top row. In the bottom row, Pearson correlations with SSTA (*1*) and DEOF/DPC1 are simultaneous with the monsoon and premonsoon season (MAM]JA), whereas the SSTA patterns for DEOF/DPC4 are for the previous winter (DJF) season. Only correlation values significant at 95% confidence are shown.

The remaining significant DEOF modes each account for ~6% of the variance in the reconstructed field since 1300 C.E. For instance, DEOF4 (Fig. 3) is a distinct pattern with strong positive loadings over the eastern Tibetan Plateau. The time series expansion of this mode is positively correlated with eastern equatorial SST anomalies and trends strongly toward more positive PDSI values during the 20th century, suggesting that warm cold tongue SSTs lead to increased moisture availability over the eastern Tibetan Plateau. This finding is consistent with both observations and modeling (*27*, *28*) that show increasing snow accumulation and significant correlations with ENSO variability. Whereas the correlations of the distinct modes with SSTs can only be calculated over the available historical period since 1856 (*1*), the DEOFs are based on the full-field reconstructions since 1300 C.E. and represent large-scale patterns of coherent spatiotemporal covariance that characterize the monsoon region back to the late Medieval period.

The further utility of the MADA for analyzing hemisphere-scale Pacific basin climate dynamics is illustrated in Fig. 4. The late Victorian Great Drought (*18*) (1876 to 1878, Fig. 2D) was characterized by monsoon failure and drought over India and Southeast Asia. Simultaneously, parts of western North America experienced similar anomalously dry conditions, whereas Mexico and the Pacific Northwest were abnormally wet. Although there were persistent mean cold tongue SST warm anomalies during 1876 and 1878 of at least +2°C, this pattern is not the canonical result of a strong eastern Pacific ENSO event (*29*). This may reflect the influence of warm SST anomalies

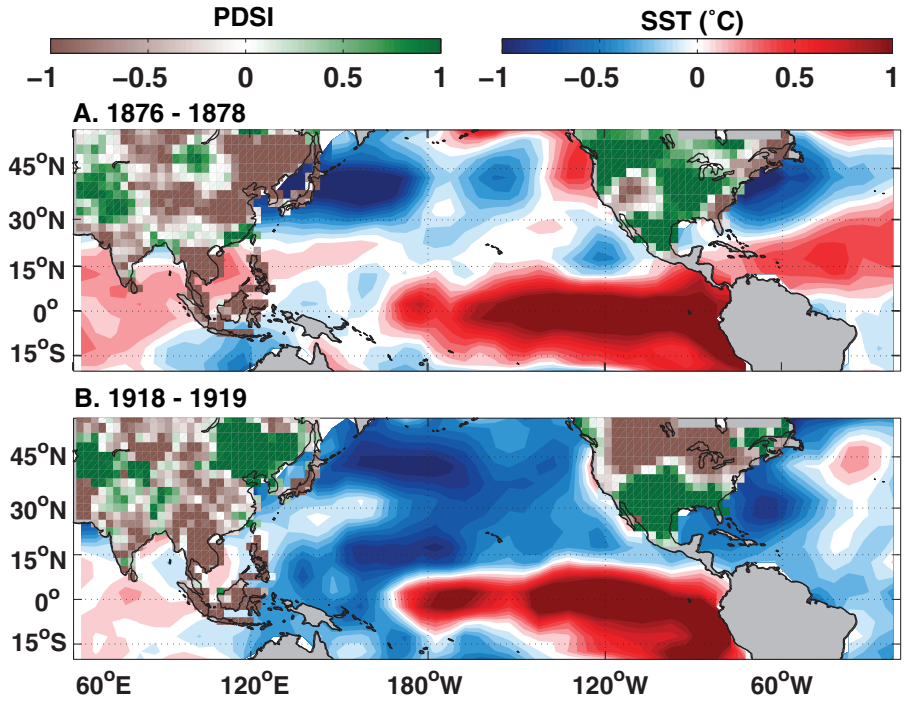

Fig. 4. Pan Pacific drought patterns during (**A**) the Great Drought (1876 to 1878) (*18*) and (**B**) the 1918 to 1919 ENSO event (*30*). During the Great Drought (A), PDSI values are strongly negative (terrestrial, brown-green colormap) over south and Southeast Asia and the Great Basin of North America. Pluvial conditions are reconstructed over the Mexican sector of the North American monsoon region, the Pacific Northwest, and the Tibetan Plateau. The post–World War I drought (B) shows pluvial conditions over southern North America and drought to the North, whereas in Asia drought dominates in India and Southeast Asia and southeastern China. Both trans-Pacific Basin drought patterns were associated with a strong El Nino event (°C, marine, blue-red colormap) with characteristic positive SST anomalies in the eastern equatorial Pacific (*1*); however, the 19th-century drought has strong positive anomalies over the tropical Atlantic and North Pacific anomalies characteristic of the positive phase of the PDO. The early–20th-century drought shows cold anomalies in both the Atlantic and North Pacific.

in the northeastern Pacific, warm SSTs in the tropical Atlantic, and an extratropical North Pacific typical of the Pacific Decadal Oscillation (PDO).

The 1918 to 1919 El Niño event following the end of World War I is also included as an example in Fig. 4 because of renewed interest in reclassifying its magnitude and global impact (*30*). As compared to the 1876 to 1878 Great Drought, this El Niño event featured canonical wet conditions over the southwestern United States and dry conditions in mainland monsoon Asia and the northern part of North America. This event is associated with a more equatorially constrained SST anomaly pattern, less warming over the Indian Ocean, and cold SSTs in both the Atlantic and North Pacific, which may explain some of the differences between its impact over Asia and North America as compared to the 1876 to 1878 event.

The long-term spatiotemporal modes of Asian monsoon variability are each associated with distinct, but not orthogonal, SST patterns. This result alone suggests that a simple canonical form of ENSO influence is insufficient to explain Asian monsoon variability, and that several spatial "flavors" of forcing exist. For example, the positive trend in moisture evident in DEOF4 in the late 20th century in north central Asia (Fig. 3) suggests an increase in snowfall and soil moisture over the Tibetan Plateau that is consistent with observations (*27*), whereas drier conditions are observed over south and Southeast Asia (DEOF1) particularly since the 1970s. Tropical drought concurrent with apparent increases in winter-spring moisture over the Plateau may therefore be evidence of the different pathways through which Pacific Ocean climate anomalies interact with different components of the monsoon (*28*), and indeed these two modes are inversely related at multidecadal and longer time scales (*1*) ($N = 706$, >30 years, $r = -0.34$, $P = 0.034$; >40 years, $r = -0.40$, $P = 0.015$).

In addition to the long-term context it provides for modern observed variability in Asian climate, the MADA provides critically important targets for climate models to hindcast the spatiotemporal fingerprint and magnitudes of reconstructed monsoon failures over the past millennium in response to forced and internal dynamics. This should allow us to develop a more in-depth, dynamically consistent understanding of Asian monsoon behavior and its global impacts, with improved predictive skill for the future.

References and Notes

1. Materials and methods are available as supporting material on *Science* Online. The Monsoon Asia Drought Atlas is available at http://iridl.ldeo.columbia.edu/SOURCES/.LDEO/.TRL/.MADA/.
2. R. H. Kripalani, J. H. Oh, A. Kulkarni, S. S. Sabade, H. S. Chaudhari, *Theor. Appl. Climatol.* **90**, 133 (2007).
3. G. Vecchi, A. Clement, B. Soden, *EOS* **89**, 81 (2008).
4. J. T. Overpeck, J. E. Cole, *Nature* **445**, 270 (2007).
5. M. Ashfaq *et al.*, *Geophys. Res. Lett.* **36**, L01704 (2009).
6. K. K. Kumar, B. Rajagopalan, M. Hoerling, G. Bates, M. Cane, *Science* **314**, 115 (2006).
7. G. A. Meehl, A. Hu, *J. Clim.* **19**, 1605 (2006).
8. N. Abram, M. Gagan, J. Cole, W. Hantoro, M. Mudelsee, *Nat. Geosci.* **1**, 849 (2008).
9. L. Thompson *et al.*, *Proc. Natl. Acad. Sci. U.S.A.* **103**, 10536 (2006).
10. A. Sinha *et al.*, *Geophys. Res. Lett.* **34**, L16707 (2007).
11. P. Wang *et al.*, *Quat. Sci. Rev.* **24**, 595 (2005).
12. R. Grove, *Mediev. Hist. J.* **10**, 75 (2007).
13. A. Dai, K. Trenberth, T. Qian, *J. Hydrometeorol.* **5**, 1117 (2004).
14. E. R. Cook, R. Seager, M. A. Cane, D. W. Stahle, *Earth Sci. Rev.* **81**, 93 (2007).
15. R. Seager *et al.*, *J. Clim.* **21**, 6175 (2008).
16. J. B. Parsons, *The Peasant Rebellions of the Late Ming Dynasty* (Univ. of Arizona Press, Tucson, AZ, 1970).
17. V. Lieberman, *Strange Parallels: Southeast Asia in Global Context, C. 800-1830*, vol. 1, *Integration on the Mainland* (Cambridge Univ. Press, Cambridge, 2003).
18. M. Davis, *Late Victorian Holocausts: El Niño Famines and the Making of the Third World* (Verso, London, 2001).
19. C. Shen, W.-C. Wang, Z. Hao, W. Gong, *Clim. Change* **85**, 453 (2007).
20. B. M. Buckley, K. Palakit, K. Duangsathaporn, P. Sanguantham, P. Prasomsin, *Clim. Dyn.* **29**, 63 (2007).
21. M. Sano, B. M. Buckley, T. Sweda, *Clim. Dyn.* **33**, 331 (2009).
22. R. P. D. Walsh, R. Glaser, S. Militzer, *Int. J. Clim.* **19**, 1025 (1999).
23. L. G. Thompson *et al.*, *Science* **289**, 1916 (2000).
24. K. Duan, T. Yao, L. G. Thompson, *J. Geophys. Res.* **111**, D19110 (2006).
25. D. Dommenget, *Clim. Dyn.* **28**, 517 (2007).
26. B. M. Buckley *et al.*, *Proc. Natl. Acad. Sci. U.S.A.* 10.1073/pnas.0910827107 (2010).
27. J. I. Goes, P. G. Thoppil, H. R. Gomes, J. T. Fasullo, *Science* **308**, 545 (2005).
28. J. Shaman, E. Tziperman, *J. Clim.* **18**, 2067 (2005).
29. R. Seager, Y. Kushnir, C. Herweijer, N. Naik, J. Velez, *J. Clim.* **18**, 4068 (2005).
30. B. S. Giese, G. P. Campo, N. C. Slowey, P. D. Sardeshmukh, J. A. Carton, *Bull. Am. Meteorol. Soc.* **91**, 177 (2010).

31. We thank all of our collaborators and contributors (see table S1 for a detailed list) for helping to make the MADA a reality. We also thank two anonymous reviewers for constructive comments and criticisms that improved this paper. This research has been supported by the U.S. National Science Foundation Paleoclimate Program, award ATM 04-02474. Lamont-Doherty Earth Observatory Contribution No. 7344.

Supporting Online Material

www.sciencemag.org/cgi/content/full/328/5977/486/DC1
Materials and Methods
Figs. S1 to S9
Table S1
References

25 November 2009; accepted 18 March 2010
10.1126/science.1185188